

Materials Advances

Accepted Manuscript

This article can be cited before page numbers have been issued, to do this please use: S. Masuda, Y. Harashima, T. Takayama, S. Takasuka and M. Fujii, *Mater. Adv.*, 2025, DOI: 10.1039/D5MA00220F.



This is an Accepted Manuscript, which has been through the Royal Society of Chemistry peer review process and has been accepted for publication.

Accepted Manuscripts are published online shortly after acceptance, before technical editing, formatting and proof reading. Using this free service, authors can make their results available to the community, in citable form, before we publish the edited article. We will replace this Accepted Manuscript with the edited and formatted Advance Article as soon as it is available.

You can find more information about Accepted Manuscripts in the [Information for Authors](#).

Please note that technical editing may introduce minor changes to the text and/or graphics, which may alter content. The journal's standard [Terms & Conditions](#) and the [Ethical guidelines](#) still apply. In no event shall the Royal Society of Chemistry be held responsible for any errors or omissions in this Accepted Manuscript or any consequences arising from the use of any information it contains.

COMMUNICATION

Utilization of Neural Network Potential for Finding Perovskite-Type Metal Oxide Photocathodes Capable of Producing HydrogenShuya Masuda,^{a,b} Yosuke Harashima,^a Tomoaki Takayama,^{a*} Shogo Takasuka^a and Mikiya Fujii^{a*}Received 00th January 20xx,
Accepted 00th January 20xx

DOI: 10.1039/x0xx00000x

Metal-oxide based photoelectrodes are promising candidates for water splitting due to their stability, but there is a lack of photocathodes. We proposed a method for finding photocathodes by utilizing neural network potential, leading to experimentally discovering a new PrCrO₃ photocathode capable of photoelectrochemically producing hydrogen in aqueous solution.

Photoelectrochemical cells are promising candidates for useful devices to generate hydrogen by splitting water using photon energy.^{1–4} Such a cell consists of a photocathode and a photoanode. Photocathodes have a role for hydrogen production, and must possess p-type semiconductor property. On the other hand, photoanodes work for oxygen production, and their semiconductor property shall be n-type. As candidate materials for the photocathodes and the photoanodes, metal oxides are preferable to other inorganic materials such as metal sulfides because of their ease of the synthesis and their stability under the water-splitting conditions.⁵ However, most metal oxide semiconductors have n-type properties due to the easy formation of oxygen defects during their synthesis processes.^{6, 7} This situation leads to the difficulty of experimentally discovering p-type metal oxide semiconductors. For solving this problem, it is essential to establish a methodology to determine the likelihood that a metal oxide is p-type *in silico*. This methodology will facilitate the experimental discovery of new p-type metal oxide semiconductors, resulting in acceleration of the progress in the photoelectrochemical water splitting.

Density functional theory (DFT) calculations have been frequently used to distinguish the semiconductor properties of metal oxides.^{8–11} These DFT-based methods can predict p-type and n-type

with high accuracy, and the explanations based on electronic states are understandable. However, in order to facilitate experimental discovery of the p-type semiconductor materials, it is desirable to establish another methodology involved with more experimentally understandable insights such as the equilibrium theory. In terms of facilitation, the fact that the DFT-based methods using hybrid functionals are somewhat time-consuming is another concern.

In the context of the aforementioned paragraphs, interdisciplinary studies of materials science and information science have gathered increasing attention for efficiently designing inorganic materials including photocatalysts for water-splitting.^{12, 13} Here, we combined insights from defect chemistry in materials science with the computational efficiency of neural network potential (NNP) to determine the likelihood that a metal oxide is p-type *in silico*. According to defect chemistry, comparison of formation energies of defects in crystal structures sheds light on the potential of metal oxides to become p-type. Specifically, the predominant formation of vacancy defects at the sites of metal cations, V_M , results in a p-type semiconductor property,¹⁴ whereas the formation of vacancy defects at the sites of oxygen anions, V_O , results in an n-type.¹⁵ Therefore, it is vital to estimate the formation energy of the defects for discrimination of the p-type semiconductor properties of the metal oxides from the n-type ones with a high-throughput computation. However, conventional DFT calculations for the exhaustive estimations of the defect energies frequently suffer from the time-consuming procedures. To advance this situation of the computational materials designs, we focused on the NNP that is expected to be an alternative high-throughput computational technique to the DFT calculations.^{16–18} The NNP is a machine learning method that predicts interatomic potentials. The use of interatomic potentials allows faster structure optimization by calculating atomic forces from energy derivatives with respect to atomic coordinates. Recently, the NNP has applied to designing of inorganic materials, for example in catalysis,^{19,20} batteries,^{21,22} glasses,²³ and semiconductors.²⁴ In defect chemistry, the NNP has been used to study various defects, including vacancies,²⁵ dopants,²⁶ complex defects,²⁷ and surface defects.²⁸

^a Graduate School of Science and Technology, Division of Materials Science, Nara Institute of Science and Technology, Nara 630-0192, Japan.

^b Digital Transformation Laboratory, Sumitomo Electric Industries Ltd., Osaka 554-0024, Japan.

The corresponding author (*): takayama.tomoaki@ms.naist.jp and fujii.mikiya@ms.naist.jp

† Footnotes relating to the title and/or authors should appear here. Electronic supplementary information (ESI) available: [details of any supplementary information available should be included here]. See DOI: 10.1039/x0xx00000x



In this study, we report on the effectiveness of NNP for extracting a new photocathode from a metal oxide database. First, we extracted 65 crystal structures of perovskite-type metal oxides from the Materials Project database.²⁹ Second, we labeled information on the semiconductor properties (*i.e.*, p- or n-type) of the extracted 65 compounds were gathered from 38 references. The criteria for data extraction and the references collected are described in the electronic supporting information (ESI). Hereafter, the gathered information is called "Label". Then, we calculated the formation energies of the defects of the metal cations and oxygen anions in the metal oxides using NNP. In addition, a subset of the metal oxides underwent DFT calculations to ascertain the reliability of the NNP. After that, we investigated the relationship between the calculated defect energies using the NNP and their Label (p-type or n-type). Consequently, it was determined that the formation energy of the defects provide a readily comprehensible indicator from the perspective of physical chemistry, facilitating the classification of semiconductor characteristics. Finally, we experimentally discovered a new metal oxide photocathode upon accordance with the classifier based on the investigated relationship.

Prior to the application of the NNP to the estimation of the formation energies of the defects of the metal cations and oxygen anions in the 65 metal oxides extracted from the Materials Project database metal oxides (see the ESI for the details), the deviation of the NNP from the DFT was evaluated. Matlantis^{30,31} was used for the NNP calculations, and VASP³² was used for the DFT calculations. The detailed calculation conditions are described in the ESI. We focused on the differences of the energies between the perfect crystal structures and the corresponding defect-contained structures obtained by NNP and DFT. The energies exhibited a tendency to be proportional, as evidenced by the determination coefficient of 0.95 (see Fig. S1). It is noteworthy that the training data of the NNP in Matlantis does not include complex metal oxides, such as perovskite structures.³⁰ This is most likely because the training data of the NNP include many kinds of polyhedral units that can be regarded as the building unites of the perovskites consisting of the metal cations and

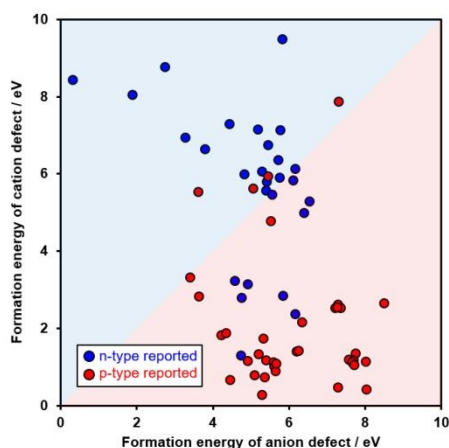


Fig. 1. The classification of the Labels (p- and n-types) on the basis of the formation energies of the cation and anion defects. These energies of the extracted metal oxides (65 compositions) were estimated by NNP. The red and blue circles indicate the compositions experimentally reported as p-type and n-type, respectively. In an ideal situation, the circles filled with red (blue) would be located within the region filled with red (blue).

oxygen anions. Therefore, it could be concluded that the NNP can be used as the alternative to the DFT for estimating the formation energies of the defects. A comparison of NNP with other functionals of DFT was summarized in Fig. S2 of the Supporting Information.

The relationship between the formation energies of the defects estimated by the NNP in the extracted metal oxides (65 compositions) and their Labels are evaluated as shown in Fig. 1 and Table 1. Note that we estimated the formation energies of the defects according to Eq. (1) on the ESI. Before getting into the evaluation, brief interpretations of the Fig. 1 and Table 1 are provided. Displaying the classification criterion defined above again, predominant defect formation of metal cations results in a p-type semiconductor property,¹⁴ whereas an increase in defect formation of oxygen anions results in an n-type.¹⁵ Therefore, in the Fig. 1, if a metal oxide is plotted in the red-filled region, the metal oxide is classified as p-type. For classifying as n-type, its plot is located within the blue-filled region. Blue-closed circles indicate the n-type Labels, and red-closed circles indicate the p-type Labels. Ideally, the red-closed circles would be located within the red-filled region. Contrary, the blue-ones would be within the blue-filled region. In addition, accuracy, precision, and recall metrics of the typical assessment criteria in informatics are summarized in Table 1. To return to the discussion, the evaluations of the Fig. 1 and Table 1 are summarized as follows. The accuracy of the overall classification of both Labels was 75%. For the p-type, precision and recall were 73% and 89%, respectively. This high recall value indicates that the proposed method can efficiently classify p-type oxides. Meanwhile, for the n-type, precision and recall were 80% and 57%, respectively. The reason why the recall of n-type was moderate would be deviation of calculation conditions of NNP from experimental conditions. Oxygen defects become more favorable at higher temperatures due to endothermic process to release the O₂ molecules into gas-phase from crystal structures. Therefore, it could happen that a material computationally (namely, at 0 K) classified as p-type exhibits n-type behavior experimentally due to experimental preparation at high temperature. In this section, it could be concluded that the relationship between the formation energies of the defects is a potent classifier for determining the likelihood that a metal oxide is p-type *in silico*.

We examined the effectiveness of the classifier for experimentally finding photocathodes. This is because metal oxides possessing p-type semiconductor properties could be applied to photocathodes. Among the 65 metal oxides shown in Fig. 1, 12 metal oxides were selected for the examination from the standpoint of the

Table 1. Summary of Classification Results.

		Classified Data		
		p-type	n-type	
Real Data	p-type	33	4	Recall 89%
	n-type	12	16	Recall 57%
		Precision 73%	Precision 80%	Accuracy 75%



experimental synthesizability in the adopted solid-state reaction. The detailed solid-state reaction conditions are described in the ESI. Among the selected 12 metal oxides, the 3 metal oxides (CaSnO_3 , SrSnO_3 , and SrTiO_3) had been reported as n-type, whereas the other 9 metal oxides had been reported as p-type. Their photoelectrochemical properties were measured using a typical three-electrode-type cell in an aqueous K_2SO_4 electrolyte contained with a phosphate buffer (pH7) saturated with O_2 . This O_2 gas was used as the electron scavenger to easily observe the cathodic photoresponse.

Fig. 2 shows the experimental validation of the likelihood that the selected metal oxides are p-type. In an ideal, the 9 metal oxides plotted within or near the red area show not anodic but cathodic photoresponses. Firstly, by paying attention to the 9 metal oxides plotted within or near the red area, the 2 metal oxides (LaCrO_3 and PrCrO_3 , their X-ray diffractions are shown in Fig. S3) exhibited cathodic photoresponses under ultraviolet (UV) light irradiation, as shown by the red-closed circles. Contrary to the expectations, the other 7 metal oxides exhibited anodic photoresponses (red-open circles). Secondly, the CaSnO_3 , SrSnO_3 , and SrTiO_3 classified as n-type predictably yielded anodic photoresponses (blue-closed circles). The discrepancy between the classification and the experimental results as represented with the red-open circles could be explained as follows. From the standpoint of experiments about metal oxides, the higher calcination temperature is, the easier oxygen is released from metal oxides. Taking SrFeO_3 as an example, it is observed that if the calcination temperature exceeds 400°C , the number of oxygen defects increases.³³ In addition, metal oxides with a high oxygen deficiency are generally n-type.¹⁵ By returning attention to our experiments, we used high-temperature calcination (1150°C) for solid-state reactions in air because of the simplicity of synthesis. This calcination temperature was higher than the synthesis temperatures (e.g., 200°C) reported in the literature that we collected (38 papers listed on the ESI). Therefore, our experimental conditions were

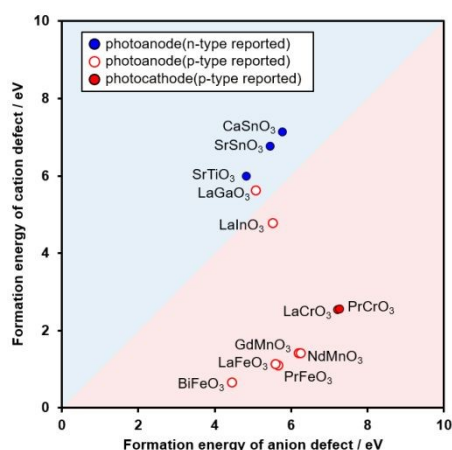


Fig. 2. Photoelectrochemical measurement results for metal oxides synthesized by solid-state reaction. The blue-closed(red-closed) circles indicate that their observed photoanodic(photo-cathodic) properties were consistent with their n-type(p-type) semiconductor properties experimentally recorded in the literature. In contrast, the red-open circles indicate inconsistency between their observed photoanodic properties with their p-type semiconductor properties recorded in the literature.

concluded to be prone to generating the defects of the oxygen anions as compared to those of the collected literature from the viewpoint of the experimentally thermodynamic equilibrium. Nevertheless, LaCrO_3 and PrCrO_3 exhibited photocathodic properties. This is due to the durability against the defect formation of the oxygen anions as expected in Fig. 2. Specifically, the formation energies of the anion defect in LaCrO_3 and PrCrO_3 were the two highest energies among the 12 compositions that we synthesized. Importantly, to the best of our knowledge, there is no report that PrCrO_3 provides a cathodic photoresponse. Thus, it could be concluded that the relationship between the formation energies of the defects of the metal cations and oxygen anions estimated by NNP is a potent guideline for determining the likelihood that a metal oxide is a photocathode *in silico*.

PrCrO_3 photocathode further underwent photoelectrochemical hydrogen production reaction. PrCrO_3 thin film (its X-ray diffraction is shown in Fig. S4) was additionally prepared using a spin-coat method (see ESI for the details) instead of solid-state reaction due to generally superior experimental performances of thin film photocathodes to particulate-based photocathodes. Cross-sectional scanning electron microscopy (SEM) was conducted using a PrCrO_3 photocathode (Fig. S5). FTO substrate was covered with a thin film. The thickness was approximately 100 nm. SEM with energy-dispersive X-ray spectroscopy (SEM-EDX) was additionally conducted

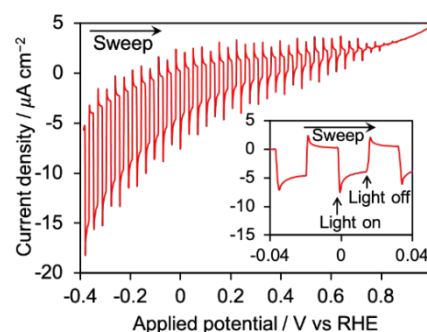


Fig. 3. Linear sweep voltammogram of PrCrO_3 thin film photocathode. The inset figure is the magnified one around 0 V vs RHE. Light source: a 300 W Xe-arc lamp ($\lambda > 300$ nm), electrolyte: an aqueous K_2SO_4 solution containing phosphate buffer (pH7) saturated with Ar, electrode area: ca. 1 cm^2

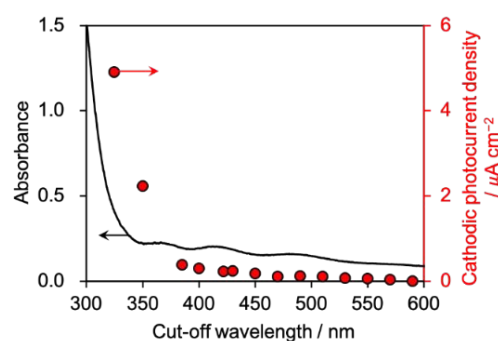


Fig. 4. Dependence of the cathodic photocurrent density of PrCrO_3 thin film photocathode on the cut-off wavelength of the incident light. Light source: a 300 W Xe-arc lamp equipped with the corresponding cut-off filters (namely, long pass filters), electrolyte: an aqueous K_2SO_4 solution containing phthalates buffer (pH4) saturated with Ar, applied potential: -0.4 V vs RHE, electrode area: ca. 1 cm^2 .



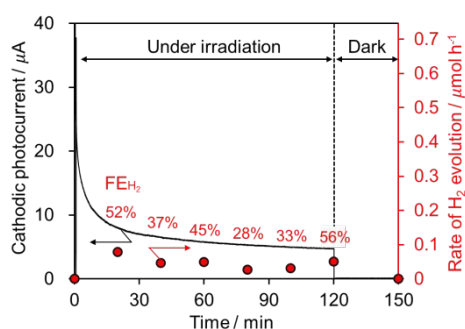


Fig. 5. Photoelectrochemical H₂ production using PrCrO₃ thin film photocathode under UV irradiation. Light source: a 300 W Xe-arc lamp ($\lambda > 300$ nm), electrolyte: an aqueous K₂SO₄ solution containing phosphate buffer (pH7) saturated with Ar, applied potential: 0 V vs RHE, electrode area: ca. 6 cm².

(Fig. S6). Elemental maps of Pr, Cr, and O were clearly recorded in addition to Si, Sn. The overlay of these maps indicated that the observed thin film was composed of Pr, Cr, and O. Fig. 3 shows linear sweep voltammogram of the PrCrO₃ thin film photocathode. An aqueous electrolyte containing phosphate buffer (pH7) saturated with Ar instead of O₂ was used. Cathodic photocurrent was clearly observed when the PrCrO₃ thin film photocathode was irradiated with UV light (namely, “Light on” in the inset of Fig. 3). Contrary, such a cathodic photocurrent was immediately disappeared under dark (namely, “Light off” in the inset of Fig. 3). The details of the voltammogram is shown in Fig. S7. Mott-Schottky analysis indicated that the flat-band potential of a PrCrO₃ photocathode was ca. +0.7 V vs RHE (Fig. S8). This flat-band potential was relatively more positive, for example, than that of Cu₂O (e.g., +0.55 V vs RHE).³⁴ The positive flat-band potential is desirable for construction of a photoelectrochemical cell as discussed in the latter section. According to the Mott-Schottky plots, carrier concentration of the PrCrO₃ photocathode was estimated to range from 1.1×10^{14} to 3.2×10^{15} cm⁻³, when the dielectric constant of PrCrO₃ was assumed to be the same as literature (from 1000 to 30000 F/m).^{35, 36}

Fig. 4 shows the dependence of the cathodic photocurrent on the cut-off wavelengths of the irradiation lights. The time-course of the wavelength-dependences is provided in Fig. S9. The onset of the photocurrent was near ~400 nm of the cut-off wavelength. Such an onset indicated that the observed photocurrents were obtained by the band gap excitation of PrCrO₃ rather than d–d transition of Cr ions attributed to the absorption of visible light.³⁷ Fig. 5 shows the photoelectrochemical hydrogen production using the PrCrO₃ thin film photocathode under UV light irradiation. The applied potential was 0 V vs RHE. Its cathodic photocurrent was recorded until 120 min under UV light irradiation, whereas the photocurrent was negligible under dark again. Most importantly, H₂ was continuously detected during UV light irradiation, meanwhile H₂ was not detected under dark. These results indicated that the observed cathodic photocurrent was consumed for H₂ production at 0 V vs RHE in an aqueous neutral electrolyte. Faradaic efficiency for H₂ production (FE_{H₂}) on the PrCrO₃ photocathode was estimated at each of the sampling points, resulting in the averaged Faradaic efficiency of 42%. The reason the FE_{H₂} was below 100% is most likely the small amounts of H₂ gas against the limit of quantification (namely, an experimental error). It is noteworthy that a tandem cell consisting of a PrCrO₃

photocathode and a CoO_x/BiVO₄:Mo photoanode gave photocurrents under simulated sunlight irradiation without external electronic voltage (Fig. S10). This is because of clear overlap between onsets of photocurrents of a PrCrO₃ photocathode and a CoO_x/BiVO₄:Mo photoanode (Fig. S11). Thus, we successfully unveiled that PrCrO₃ was a new photocathode capable of producing H₂ utilizing UV light in accordance with the classification. Although PrCrO₃ primarily responds to ultraviolet light, its performance could be improved by doping to increase carrier concentration and enhance visible light absorption. Our finding based on NNP is expected to be beneficial for assessments of the doped structures.

Conclusions

We established a method combining insights of defect chemistry with the computational efficiency of NNP to extract metal oxide photocathodes with the perovskite-type crystal structures from the Materials Project of an inorganic materials database. The deviation of the formation energies of the defects of the metal cations and oxygen anions estimated by NNP from those estimated by DFT is fairly small in the representatives of the extracted metal oxides, indicating reliance of NNP in the estimations instead of DFT. Estimation of the formation energies of the defects using the NNP is effective in classifying their semiconductor properties into p- or n-types. The accuracy of the proposed classification method for the p-type and n-type labels obtained by reference was 75%. The accuracy would be improved by incorporation of finite-temperature effects into the NNP-based estimations. According to the classification, we experimentally discovered a new PrCrO₃ photocathode capable of photoelectrochemically producing H₂ utilizing UV light. This finding will accelerate the discovery of new metal oxide photocathodes for photoelectrochemical H₂ production.

Author contributions

Shuya Masuda: Data curation, Formal analysis, Investigation, Validation, Visualization, Writing – original draft. Yosuke Harashima: Conceptualization and Writing – review & editing. Tomoaki Takayama: Supervision, Conceptualization, Project administration, and Writing – review & editing. Shogo Takasuka: Supervision and Writing – review & editing. Mikiya Fujii: Supervision and Writing – review & editing.

Conflicts of interest

There are no conflicts to declare.

Data availability

The data supporting this article have been included as part of the ESI.†

Acknowledgements

We would like to thank Rie Nakashima for her assistance in materials synthesis, characterization and measurement.



Notes and references

- 1 A. Kudo and Y. Miseki, *Chem. Soc. Rev.*, 2009, **38**, 253.
- 2 R. Abe, *J. Photochem. Photobiol.*, 2010, **11**, 179.
- 3 F. E. Osterloh, *Chem. Soc. Rev.*, 2013, **42**, 2294.
- 4 T. Hisatomi, J. Kubota and K. Domen, *Chem. Soc. Rev.*, 2014, **43**, 7520.
- 5 Y. Chen, X. Feng, Y. Liu, X. Guan, C. Burda and L. Guo, *ACS Energy Lett.*, 2020, **5**, 844.
- 6 J. Robertson and Z. Zhang, *MRS Bull.*, 2021, **46**, 1037.
- 7 A. Samizo, M. Minohara, N. Kikuchi, K. Bando, Y. Aiura, K. Mibu and K. Nishio, *J. Phys. Chem. C*, 2021, **125**, 17117.
- 8 W. Li, C. F. J. Walther, A. Kuc and T. Heine, *J. Chem. Theory Comput.*, 2013, **9**, 2950.
- 9 G. Hautier, A. Miglio, D. Waroquiers, G. M. Rignanese, and X. Gonze, *Chem. Mater.*, 2014, **26**, 5447.
- 10 N. Sarmadian, R. Saniz, B. Partoens and D. Lamoen, *Sci. Rep.*, 2016, **6**, 20446.
- 11 K. Yim, Y. Youn, M. Lee, D. Yoo, J. Lee, S. H. Cho and S. Han, *Npj Comput. Mater.*, 2018, **4**, 17.
- 12 P. O. Dral, *Chem. Commun.*, 2024, **60**, 3240.
- 13 D. Chen, C. Shang and ZP. Liu, *Npj Comput. Mater.*, 2023, **9**, 2.
- 14 M. Nolan and S. D. Elliott, *Phys. Chem. Chem. Phys.*, 2006, **8**, 5350.
- 15 M. E. Seyed, R. E. Mohammad, B. A. Reza and K. Hadi, *Phys. Chem. Res.*, 2018, **6**, 547.
- 16 S. Käser, L. I. Vazquez-Salazar, M. Meuwly and K. Töpfer, *Digit. Discov.*, 2023, **2**, 28.
- 17 J. S. Smith, O. Isayev and A. E. Roitberg, *Sci.*, 2017, **8**, 3192.
- 18 T. Xie and J. C. Grossman, *Phys. Rev. Lett.*, 2018, **120**, 145301.
- 19 T. Kobayashi, D. J. Liu and F. A. Perras, *Chem. Commun.*, 2022, **58**, 13939.
- 20 T. Koyama, M. Nakayama and J. Schuett, *J. Phys. Chem. C*, 2024, **128**, 19482.
- 21 R. Iwasaki, N. Tanibata, H. Takeda and M. Nakayama, *Commun. Mater.*, 2024, **5**, 148.
- 22 W. Wang, T. Yang, W. H. Harris, and R. Gómez-Bombarelli, *Chem. Commun.*, 2020, **56**, 8920.
- 23 R. Kayano, Y. Inagaki, R. Matsubara, K. Ishida and T. Ohkubo, *J. Phys. Chem. C*, 2023, **128**, 17686.
- 24 C. Hong, S. Oh, H. An, P. H. Kim, Y. Kim, J. H. Ko, J. Sue, D. Oh, S. Park and S. Han, *ACS Appl. Mater. Interfaces*, 2024, **16**, 36, 48457.
- 25 G. V. Huerta, K. Hisama, K. Sato, K. Nagaoka and M. Koyama, *iScience*, 2025, **28**, 112470.
- 26 T. Chen, E. H. Otal, T. Q. Nguyen, S. Narumi, M. Koyama and N. Zettsu, *Chem. Mater.*, 2025, **37**, 709.
- 27 J. Bae, C. Kwon, S.-O. Park, H. Jeong, T. Park, T. Jang, Y. Cho, S. Kim and S. Choi, *Sci. Adv.*, 2024, **10**, eadm7221.
- 28 B. G. Son, C. Kwon, Y. Cho, T. Jang, H. R. Byon, S. Kim and E. S. Cho, *ACS Appl. Mater. Interfaces*, 2024, **16**, 32259.
- 29 A. Jain*, S. P. Ong*, G. Hautier, W. Chen, W. D. Richards, S. Dacek, S. Cholia, D. Gunter, D. Skinner, G. Ceder and K. A. Persson (*=equal contributions), *APL Mater.*, 2013, **1**, 011002.
- 30 S. Takamoto, C. Shinagawa, D. Motoki, K. Nakago, W. Li, I. Kurata, T. Watanabe, Y. Yayama, H. Iriguchi, Y. Asano, T. Onodera, T. Ishii, T. Kudo, H. Ono, R. Sawada, R. Ishitani, M. Ong, T. Yamaguchi, T. Kataoka, A. Hayashi, N. Charoenphakdee and T. Ibuka, *Nat. Commun.*, 2022, **13**, 2991.
- 31 Matlantis, Preferred Computational Chemistry, Inc., <https://matlantis.com/> (accessed Jun 10, 2024).
- 32 G. Kresse and J. Furthmüller, *Phys. Rev. B*, 1996, **54**, 11169.
- 33 K. Shido, T. Yoshino, S. Hatano, M. Matsuo and Hashimoto, *Interactions*, 2024, **245**, 299.
- 34 D. Jeong, W. Jo, J. Jeong, T. Kim, S. Han, M.-K. Son and H. Jung, *RSC Adv.*, 2022, **12**, 2632.
- 35 R. Late, K.V. Wagaskar, P. B. Shelke, P. R. Sagdeo, *Mater. Chem. Phys.*, 2021, **252**, 124313.
- 36 B. V. Prasad, G. N. Rao, J. W. Chen, D. S. Babu, *Mater. Chem. Phys.*, 2011, **126**, 918. View Article Online
DOI: 10.1039/D5MA00220F
- 37 R. Mguedla, A. B. J. Kharrat, O. Taktak, H. Souissi, S. Kammoun, K. Khirouni and W. Boujelben, *Opt. Mater.*, 2020, **101**, 109742.



Data availability The data supporting this article have been included as Supplementary Information.

